ORIGINAL RESEARCH PAPER

Seismic monitoring of western Pacific typhoons

**Wu-Cheng Chi · Wan-Jou Chen · Ban-Yuan Kuo ·
David Dolenc**

Abstract Typhoons inflict large damage to societies, but are usually difficult to monitor in close proximity in real-time without expensive instruments. Here we study the possibility of using seismic waveforms on the seafloor and on land to monitor the turning of a far away or approaching typhoon. Up to 67% of the typhoons making landfall in Taiwan come from the eastern shore, so that we deployed broadband ocean-bottom seismometers (OBSs) offshore eastern Taiwan in 2006 to study ground motion in close proximity to a typhoon. Typhoons generate ocean waves, which generate pressure signals in the water column before being transmitted to the seafloor as seismic waves and recorded by the OBSs. The ground motions on the seafloor correlate with locally increased (ocean) wave heights and wave periods, suggesting that the ground motions are mostly induced by in situ or nearby pressure fields, as shown by coherence function analyses. When a typhoon turns and changes wave-wave interaction near the source region, a new set of *en echelon* patterns develops which can be observed by OBSs and land stations. Similar features occur when a typhoon crosses a landmass and re-enters the ocean. The energy level ratio between the single-frequency and double-frequency microseisms also changes abruptly when the typhoon turns. These features can potentially help near real-time early warning with little cost to complement other conventional typhoon early warning methods.

W.-C. Chi (✉) · B.-Y. Kuo
Institute of Earth Sciences, Academia Sinica, 128 Sec 2,
Academia Road, Nankang, Taipei 115, Taiwan
e-mail: wchi@gate.sinica.edu.tw

W.-J. Chen
Department of Earth and Atmospheric Sciences, Saint Louis
University, 3642 Lindell Blvd, St. Louis, MO 63108, USA

D. Dolenc
Large Lakes Observatory, University of Minnesota Duluth,
2205 E 5th Street, Duluth, MN 55812, USA

Introduction

Microseisms are seismic energy observed between earthquakes as continuous background "noises" of the earth (Kedar and Webb 2005; Bromirski et al. 2005; Kedar et al. 2008; Tanimoto 2008). Microseisms can be ground motions caused by storm-induced ocean waves, which have been studied from distances away from the storm (Tabulevich 1971; Sutton 1996; Suda 1998; Wilson et al. 2003; Kedar and Webb 2005; Webb 2007; Gerstoft et al. 2008; Koper and de Foy 2008; Wilson and Makris 2008).

Theoretically, for typical 0.0625 Hz ocean swells, ocean wave induced pressure in a water column decays exponentially with depth, thus it is easier to excite single frequency seismic waves in shallow water. Nonlinear wave-wave interaction regions occur where typical 0.0625 Hz ocean swells traveling from opposite directions can generate 0.125 Hz standing waves (double-frequency waves), which then couple with seafloor and propagate as

seismic waves (Longuet-Higgins 1950; Kedar and Webb 2005; Webb 2007; Gerstoft et al. 2008).

There is debate as to whether microseisms are excited mainly near coastlines in shallow water regions or if it is possible to generate microseisms in deep-sea regions. Some studies propose that ground motions are induced in shallow water regions like continental shelves (Friedrich et al. 1998; Bromirski et al. 1999; Bromirski and Duennebier 2002; Bromirski 2001; Essen et al. 2003; Rhie and Romanowicz 2006; Kedar and Webb 2005;

Table 1 Saffir-Simpson scale of hurricane intensity

Category	Pressure (hPa)	Wind (ms^{-1})	Storm surge (m)	Damage
1	>980	33–42	1.0–1.7	Minimal
2	979–965	43–49	1.8–2.6	Moderate
3	964–945	50–58	2.7–3.8	Extensive
4	944–920	59–69	3.9–5.6	Extreme
5	<920	≥70	≥5.7	Catastrophic

Fig. 1 Regional bathymetry and station location map with the track of Typhoon Shanshan. (Blue dots depict the beginning of the Julian day). Buoy marks the location of Taitung deep sea weather buoy. S002 and S004 mark the locations of the two ocean bottom seismometers. All other stations are land stations, mostly from F-net of Japan. Typhoon Shanshan moved alongside this 2,000-km seismic array, exciting interesting ground motions analyzed in this study. Stations KMI and LSA are part of the Global Seismic Network (GSN; see *inset*)
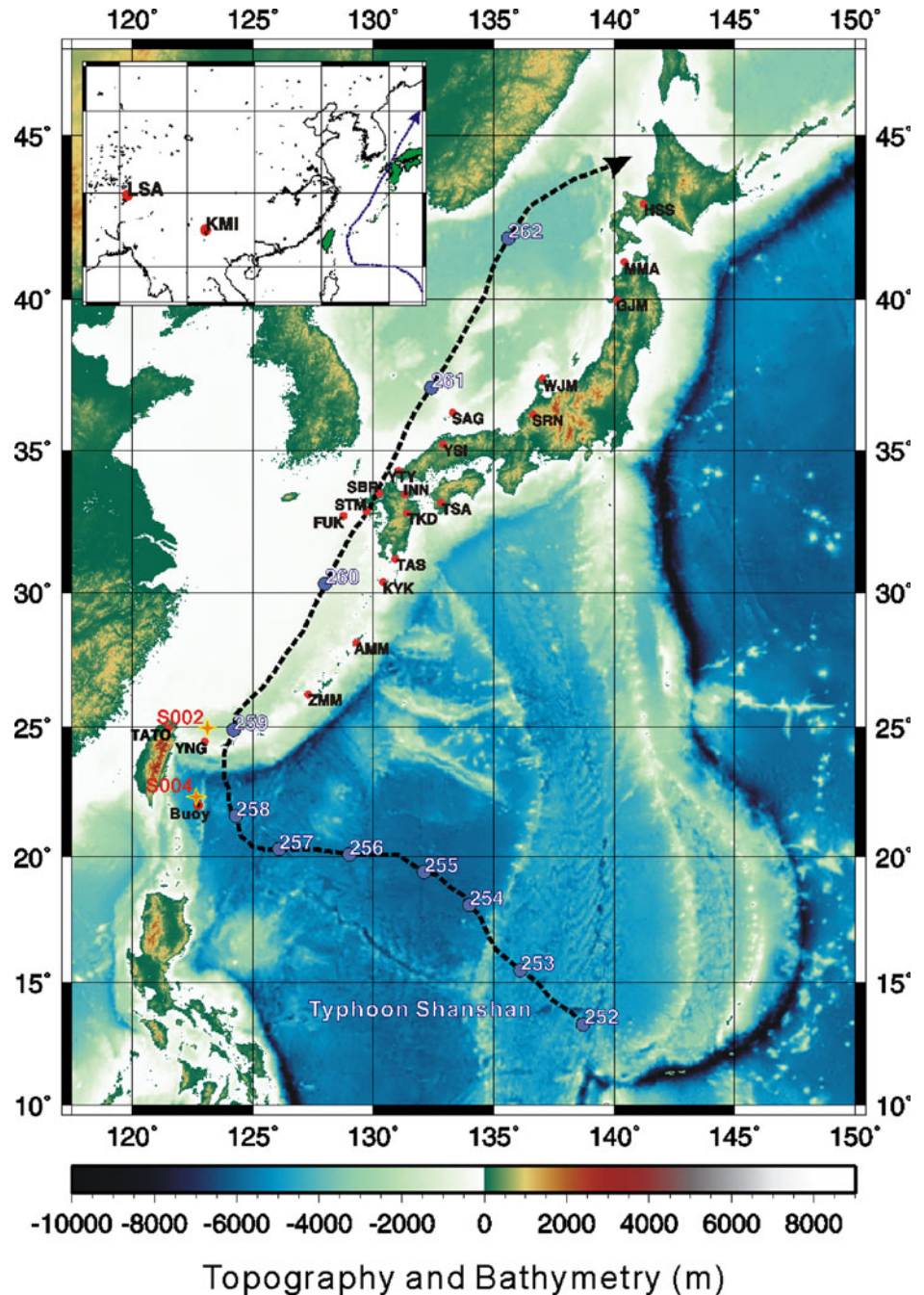
Bromirski and Gerstoft 2009). Other scientists propose that the source region is under or trailing a typhoon (Cessaro 1994; Stehly et al. 2006; Chevrot et al. 2007; Kedar et al. 2008; Gerstoft et al. 2008; Koper and de Foy 2008; Landes et al. 2010; Chi et al. 2010).

Some of the controversy might be due to different types of microseisms used in the studies (e.g. Gerstoft et al. 2006). There is strong evidence showing that some P-wave microseisms can be generated in the deep sea and reach Earth's core before being recorded on the other side of the earth (Gerstoft et al. 2008; Koper and de Foy 2008). In addition, Bromirski et al. (2005) proposed that there are two kinds of double-frequency waves: short-period double-frequency (SPDF: 0.20–0.45 Hz) microseisms which are excited locally by ocean gravity waves, and long-period double-frequency (LPDF: 0.085–0.20 Hz) microseisms that are excited near coastlines at distant locations. This interpretation is based on much higher SPDF levels compared to LPDF at H2O site in the middle of the open Pacific Ocean. Zhang et al. (2010) also argued that double frequency P wave microseisms can be excited in both deep sea and coastal regions.

So far, all these analyses are based on waveforms recorded a few thousand kilometers away from the cyclones. Waveforms observed directly under a typhoon were not available previously until now. In 2006, we deployed broadband ocean-bottom seismometers (OBSs) around offshore Taiwan for the first time. One of the OBSs was located in a region where many typhoons have turned. The seismographs recorded not only earthquake waveforms but also noises generated by winds, waves, tides and other external forces.

Here we document this unique dataset recorded by the OBSs and other on-land stations in western Pacific regions to study typhoon-induced ground motions in order to improve our understanding of how to seismically monitor a typhoon. In September 2006, Typhoon Shanshan passed over the OBSs, providing an opportunity to study how the microseisms' wave field evolves with a moving source. We also studied Typhoon Cimaron, which changed course several times during its short life span, to see if a change of course appears in the seismic record.

Typhoon Shanshan

Typhoon Shanshan, a category 4 cyclone (See Table 1 for a scale of hurricane intensity), caused at least 11 fatalities and was the third costliest hurricane (exceeding $2.5 billion) and the sixth costliest disaster worldwide in 2006 (Hoyois et al. 2007). Nevertheless, it was also recorded by high-quality broadband land seismic networks in Japan and Taiwan, which form a 3,500-km linear seismic array

Table 2 Technical specifications of the ocean bottom seismographs used for this study

Seismometer	Guralp CMG-3TC broadband three-component seismometer. Flat velocity response from 0.0083 to 50 Hz. Gimbals will level seismometer if tilt <50°
Pressure sensor	Differential Pressure Gauge V6.3 with low-frequency corner at 0.001 Hz
Digitizer	Quanterra QA330 low-power 24-bit digitizer. Dynamic range: 135 dB
	Sample rates: 1–200 Hz
Disk capacity	20 Gb
Clock	Seascan Timebase. Drift rate is <0.5 ms/day before correction and <0.1 s/year after correction
Acoustic telemetry	WHOI-built modem; capable of baud rates of 1 kbit/s or better
Recording duration	Alkaline battery pack will deliver sufficient power for 6 month operation
	Lithium battery pack will allow >12 month operation
Release	EGG 8242 commercial acoustic release. Backup burnwire acoustic release housed in dedicated 12″ glass ball
Weight/ dimensions	622/544 kg with/without anchor; 5 1/2′ × 4′ and 4′ high
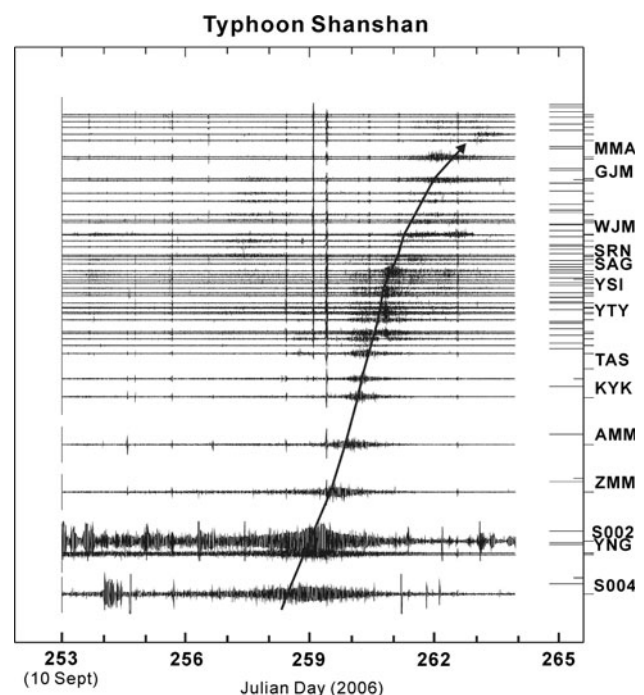
Fig. 2 Stack plot showing how Typhoon Shanshan was recorded. The *solid line* with an *arrow* marks the time when the typhoon is closest to the station. This figure suggests the major source region is moving with and trailing behind the typhoon. This figure is reproduced from Chi et al. (2010, Fig. 2)

(Fig. 1). This typhoon was chosen for this study because it passed near this seismic array and produced an excellent dataset.

Typhoon Cimaron

Typhoon Cimaron, a category 5 cyclone (Table 1), changed course several times and caused much damage to China and Hong Kong (Lang and Pierce 2006). However, it also generated many similar but more distinctive signals. In addition, it went across the Philippines, providing a rare opportunity to study the evolution of ground motions when the typhoon made landfall and reduced the wave-wave interaction region, and likewise when the typhoon re-entered the ocean and a new set of wave-wave interaction was generated. The seismic waveforms recorded during this period help us identify the unique seismic signals generated during the development of a new set of wave-wave interaction.

Taiwan wideband ocean bottom seismology (OBS) program and experiment

Starting in 2001, the Institute of Earth Sciences, Academia Sinica in Taiwan launched the first broadband OBS program in Taiwan. The first ever wideband OBS deployment offshore Taiwan was conducted in 2006. Four OBSs built in collaboration with the Woods Hole Oceanographic Institution (Collins et al. 2002) were deployed from September 2006 to July 2007 (Kuo et al. 2009; Lin et al. 2009). The OBS contains a Guralp CMT-3TC seismic sensor with flat response between 0.0083 and 20 Hz. All the waveforms were corrected for instrument response before being analyzed in this study. Quanterra Q330 is used as the data logger with a sampling rate of 40 samples per second. The sensor is leveled periodically during the deployment by a gimbal system with brakes (Thwaites et al. 2005). Table 2 gives more detailed engineering parameters of the OBSs.

Field operations were challenging but rewarding. Our communication with one OBS was lost owing to a noisy acoustic environment in the region and another OBS remained mired on the seafloor where subsequent volcanic eruptions were reported for the first time (Lin et al. 2007). Two OBSs (S002 and S004, Fig. 1) were successfully recovered from seafloor depths of 1749 m and 4726 m, respectively. They recorded unprecedented ground motions on the seafloor when typhoons passed near them. We also use data recorded by land seismometers (F-net and GSN) arrayed along the western Pacific Ocean. The OBSs and the land seismometers recorded coherent energy synchronized with typhoons (Chi et al. 2010).

Taitung deep sea buoy data

Up to 67% of the typhoons that make landfall in Taiwan do so in eastern Taiwan. To collect critical data before the typhoon makes landfall, the Central Weather Bureau (CWB) of Taiwan deployed a deep sea buoy off the eastern shore of Taiwan in August 2006. The data sets collected include wind speed, wind direction, temperature, pressure, surface water temperature, wave height, wave period, wave direction, and direction spectrum. It collects data 12 times a day, but more frequently when a typhoon is near Taiwan (Underwater Photography Association/ ETToday 2006). Such buoys provided rare but important time series at a fixed location during the month of September, 2006. The data can be extended from a point location to a much wider region using Wave Watch III models.

Wave Watch III model data

Wave Watch III (WWIII) is a hindcast system (Tolman 2005) and one of the Marine Modeling and Analysis Branch (MMAB) Operational Wave Models that consists
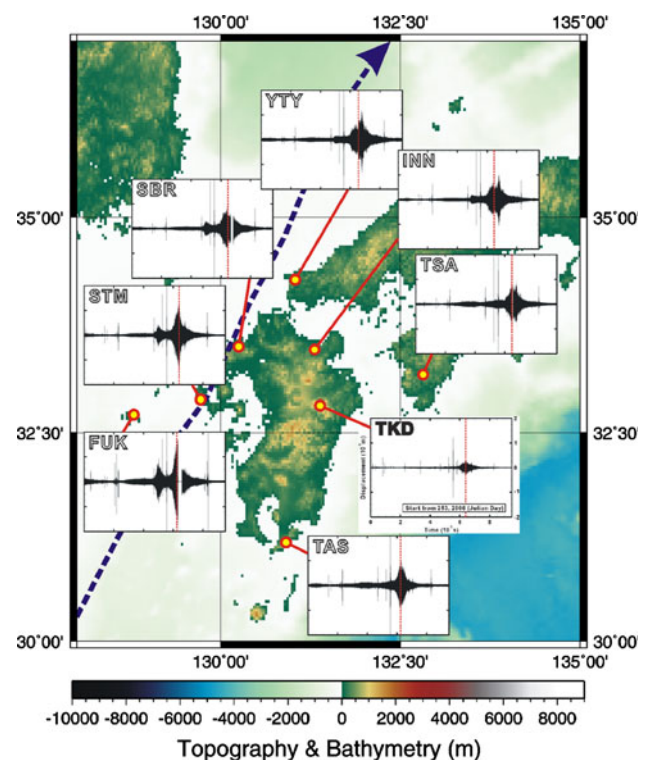
Fig. 3 Displacement waveforms recorded by OBSs and on-land stations. Coastal stations in Kyushu and Shikoku, Japan, recorded stronger ground motions compared with the inland station TKD. The *dotted lines* plotted on each displacement waveform show the time Typhoon Shanshan was closest to the station. This suggests that part of the ground motions were excited near the coast, possibly in continental shelves where the water is shallow, and that energy was attenuated after propagating inland. See TKD station for scale. The unit for time is 10^5 s for each tick; for displacement is 10^{-5} m for each tick. All waveform plots have the same scale

of global and regional nested grids. A hindcast system is a mathematical model that closely estimates past events and enters them into the model to see how well the output matches the observed results. Wave Watch III Model Data are extensively validated and cover a wide region (NOAA/NCEP et al. 2010).

Observations and data analyses

The Shanshan typhoon was recorded at the seismic stations along its course including the OBSs deployed offshore Taiwan. The OBSs were closer to the typhoon, so the signal to noise ratio was much higher in the OBS dataset than in the land stations or in any datasets previously studied. In other words, we used near-source signals in a similar fashion to strong-motion signals for earthquake source studies. The duration of an earthquake is in seconds, whereas the life span of a typhoon is in weeks; therefore, our week-long waveforms recorded signals both near and far from the typhoon.

Typhoon Shanshan lit up the seismic stations along its course (Chi et al. 2010). Analyzing both datasets of OBSs and land seismic stations in the western Pacific region, we found that the envelopes of the waves have spindle shapes with amplitude increasing as Typhoon Shanshan approached the station (Fig. 2). The maximum displacement amplitude mostly occurred not when the eye wall of the typhoon with highest wind speed was closest to the station but several hours after the center had passed. The arrival time of maximum typhoon-induced vertical displacements for each station was also consistently later than the time when the eye of the typhoon was closest to each station, which correlates with the wave-wave interaction region of a moving cyclone (Longuet-Higgins 1950; Tabulevich 1971).

Coastal stations generally recorded stronger typhoon signals than inland stations, even when a typhoon was far away (Fig. 3). Coastal stations in Kyushu and Shikoku, Japan, recorded stronger ground motions compared with the inland station TKD. This suggests that part of the ground motions was excited in shallow water regions near
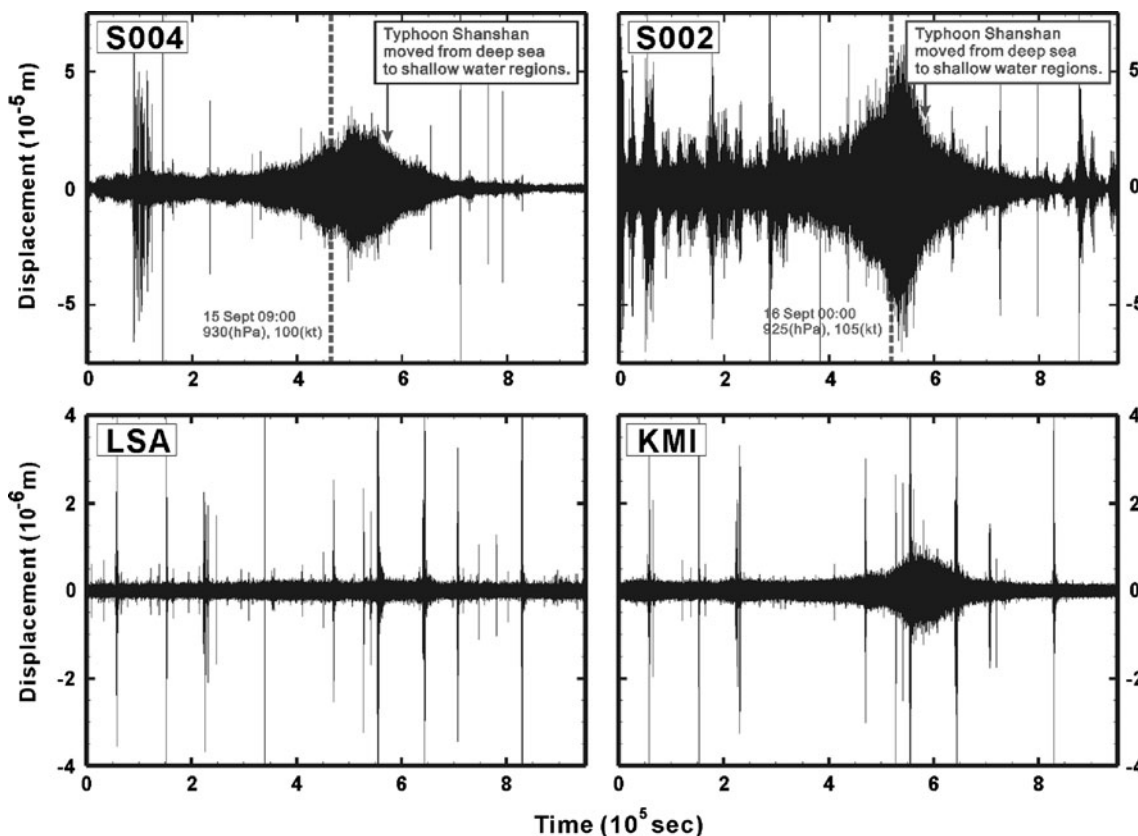
Fig. 4 The displacement waveforms recorded by OBSs S004 and S002, and the inland seismometers, LSA (Lhasa, China) and KMI (Kunming, China). The *dotted line* marks the time Typhoon Shanshan was closest to the station (The precise time, central pressure and wind speed of typhoon were marked next to the *dotted line*). The maximum displacement amplitudes occurred several hours after the center of

Typhoon Shanshan had passed. S002 at shallower water depth recorded stronger ground motions than that of S004. S002 also has more noise. We studied how far the signals of Typhoon Shanshan can propagate, and by visual inspection we found clear signals recorded at station KMI, but not at station LSA

the coast; thus, the amplitudes decayed after the waves traveled inland. By visual inspection, we can find clear typhoon related signals at station KMI (Kunming, China; 2800 km inland) but not at station LSA (Lhasa, China; Fig. 4). It is likely that advanced data processing will extend the signal detection distance.

In addition to the inland and coastal sites, we also studied ground motions on the seafloor. The OBS waveforms have higher amplitudes than those of the land waveforms. Compared with station S004, the S002 station at shallower water depth recorded stronger ground motions (bigger amplitudes) in vertical displacement waveforms (Fig. 4).

We performed spectral analyses of the OBS data and land waveforms for the period when Typhoon Shanshan was passing over the seismometers (Fig. 5). There are multiple bands of energy in the spectrograms, consistent with the results from Stephen et al. (2003) and Bromirski

et al. (2005). The 0.05–0.085 Hz band energy is recognized as single-frequency microseisms, or primary energy (e.g. Zhang et al. 2010), and the 0.1–0.5 Hz band energy is known as double-frequency, or secondary energy (Bromirski et al. 2005). The lowest frequency signals (0.05–0.085 Hz band, single-frequency microseisms) have very simple patterns and were the weakest and most narrow band among the three bands of energy. The splitting of the double frequency microseisms has been documented by Bromirski et al. (2005) and classified as short-period double-frequency (SPDF: 0.20–0.45 Hz) and long-period (0.085–0.2 Hz) double-frequency (SPDF and LPDF) bands, respectively.

Bromirski et al. (2005) propose that SPDF is generated on the seafloor locally by wind seas and the LPDF is excited by ocean waves impacting the coastline far away. Because their dataset was derived from distant storms, they needed to apply a differential scheme to enhance the

Fig. 5 Spectrograms of the typhoon-induced ground motions. Typhoon Shanshan (near field); note multiple bands of energies recorded during Typhoon Shanshan, instead of the typical single- and double-frequency microseisms. Similar patterns have previously been documented using processed waveforms collected at far distances (Bromirski et al. 2005). Bromirski et al. (2005) proposed that the double-frequency microseisms can also be classified into long-period double frequency (LPDF: 0.085–0.20 Hz) and short-period double frequency (SPDF: 0.20–0.45 Hz) bands. They also propose that LPDF microseisms are mostly excited at shallow water depth near coast, whereas SPDF microseisms are mostly excited by local wind. The *red triangle* marks the time when the typhoon was closest to the station
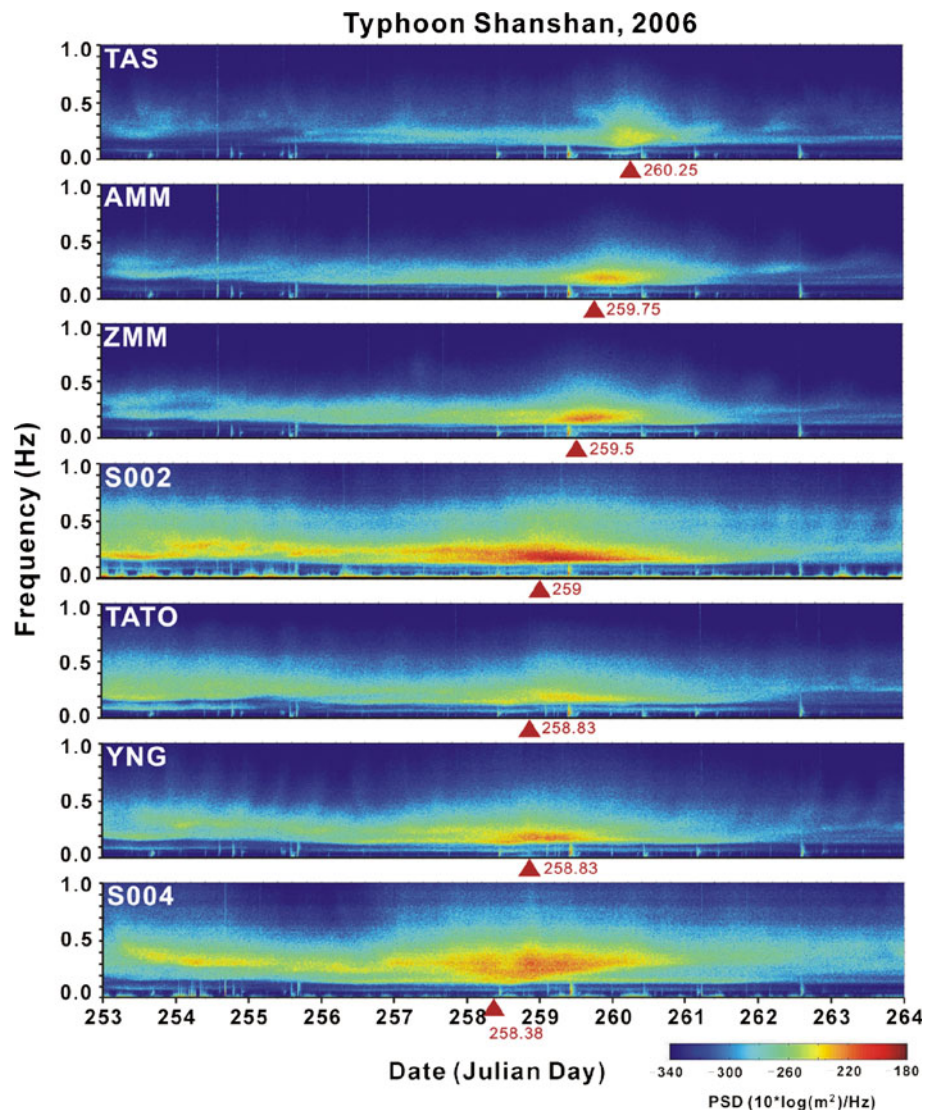
signals. In this study, the near source wavefields show clear signals without the need for additional data processing and give two similar bands of energy in the double-frequency microseisms.

When the typhoon was near the station, the frequency bands jumped back to lower frequencies before increasing again in spindle shapes (Fig. 5, and more clearly in Fig. 6). When the front wall of the eye of Typhoon Shanshan was approaching the station, the near-field stations recorded some decrease of frequency (Fig. 5). The energy level then decreased when the eye was closest to the station.

Typhoon Cimaron provided many clear ground motion patterns (Fig. 6). The far-field land station TATO recorded energy with increasing frequency until Cimaron changed its direction. The envelopes of the single-frequency band have *en echelon* patterns with increasing amplitude as the typhoon approached the station, wherein signals increased from the lower frequency region (0.04 Hz) to the higher frequency region (0.08 Hz) and jumped back to the lower frequency band. This jumping pattern occurred several times.

We compared the moments of "jumping" with the track of Typhoon Cimaron and found that the "jumping" occurred as Cimaron was passing over the island of Luzon (Fig. 6) and when it was turning. When the typhoon made landfall and passed over Luzon, the microseismic signals started to disappear. Once the typhoon re-entered the ocean, a new set of microseisms started to develop. On Julian day 305, Typhoon Cimaron stalled, and the dominant frequency shifted from 0.07 to 0.065 Hz. Starting from Julian day 306, a new set of microseisms started to develop when the typhoon turned and moved steadily to the southwest. During this period, there were several other storm systems thousands of kilometers away from this region; however, it was difficult to see their effects without more specialized data processing. For example, there are no observed microseism motions at station TATO when Typhoon Cimaron was over the island of Luzon, implying the signals from other distant cyclones were very weak compared with the signals from Typhoon Cimaron, and advanced data processing is needed to study their interaction with the strong signals induced by Cimaron. Based on global satellite imagery over this time

Fig. 6 We use Typhoon Cimaron (far field) recorded by station TATO as an example to show that when a typhoon's velocity changes or when a typhoon makes landfall and re-enters the ocean, the 10–20 s (0.05–0.1 Hz) single-frequency band shows *en echelon* patterns. The legends in the *lower panel* are the same as the ones in Fig. 1. Similar but weaker pattern can be found in Typhoon Shanshan, which did not turn as dramatically as Typhoon Cimaron
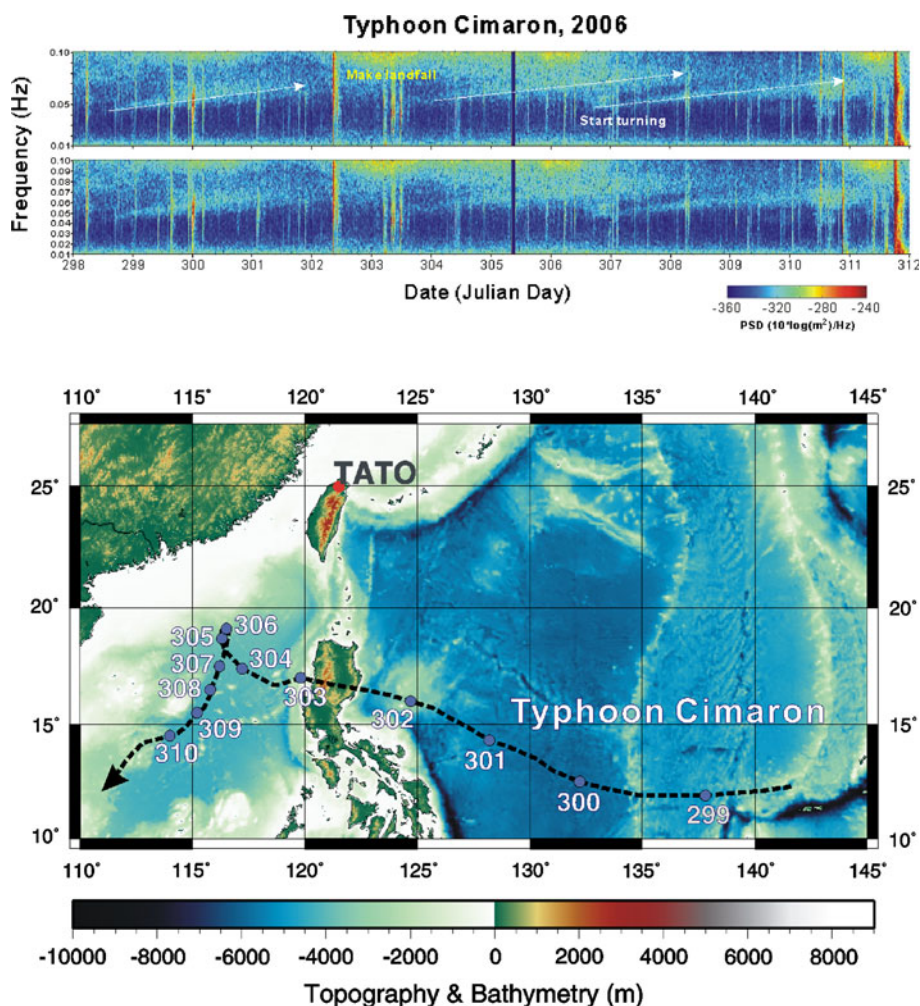
span (see supplemental materials), we did not see a new set of microseisms form at station TATO when new storms occurred from these far distances. In other words, we did not see clear evidence of the influence of distance storms, possibly owing to the large signals induced by Typhoon Cimaro nearby. In addition, the jumping features were also observed during Typhoon Shanshan as well as in other typhoons.

Overall, the 0.085–0.2 Hz (SPDF) and 0.2–0.5 Hz (LPDF) bands were the dominant energy in the wave-forms, and the frequency-shifting patterns were also observed in these two bands (Fig. 5). They were more energetic so appear to have a longer duration than that of the 0.05–0.085 Hz band.

We used WWIII model data to study the relationship between the hindcast data, deep-sea buoy data, and our seismic data. The significant wave height (SWH) and wave peak periods from WWIII show different oceanic condi-tions of western Pacific regions during the period of Typhoon Shanshan. As Typhoon Shanshan passed through the regions, the SWH of each area increased to 6–7 m. The periods of the mean ocean wave observed at the Taitung deep sea buoy are similar to that of WWIII. When Typhoon Shanshan was near S004 station, both the dominant fre-quencies and the timing of the frequency shifts in the LPDF seismic band correlate with the ocean wave periods derived from Wave Watch III models (Fig. 7) and the nearby Taitung deep sea buoy (Fig. 8).
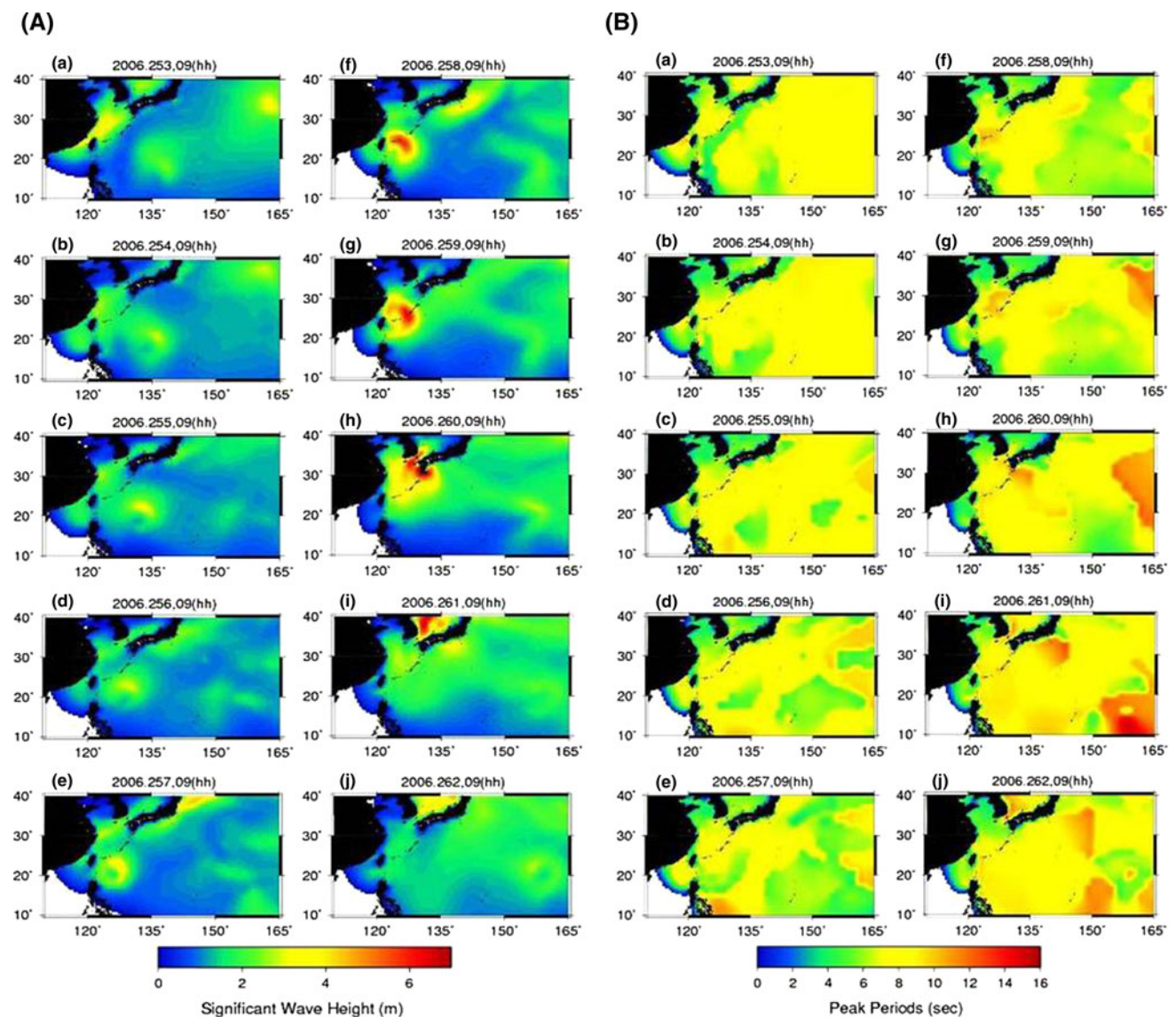
Fig. 7 Wave situations showed by Wave Watch III (WWIII) hindcast model data. In the left panels, we show the significant wave height. As Typhoon Shanshan passed through the regions, the significant wave height of each area increased to 6–7 m. In the right panels, we show the wave peak periods of WWII model data. The recorded seismic waveforms correlate with these datasets

We also studied whether the data recorded by OBS were excited by a source of near or far distance using coherence analyses, which have been used by many seafloor compliance studies to see if the ground motions on the seafloor are excited locally by the pressure waves induced by local ocean waves. We calculated the coherence as a function of frequency between pressure fields and vertical acceleration particle motions (both instrument-response corrected) recorded by OBSs S002 and S004. Here the coherence is a cross correction of two time series that has been normalized using the product of the two autocorrelations (e.g. Crawford et al. 1991; Willoughby and Edwards 1997; Crawford 2000, 2004; Willoughby et al. 2000, 2008; Willoughby 2003). Coherence, ranging from 0 to 1, quantifies the extent to which two series are related. For seafloor compliance studies, high coherence means the ground motions on the seafloor are excited by a "local" pressure field in the water column. The ground motions and the pressure fields can be used to derive "local" crustal structures. In other words, the coherence can be treated as an indicator of how close the pressure source regions are to the OBS site. Only when the coherence is high can the pressure and acceleration data be used to calculate in situ shear-wave velocity in the crust under the OBS (e.g. Yamamoto and Torii 1986; Crawford et al. 1991; Willoughby and Edwards 1997; Wang et al. 2010). Using the pressure and acceleration time series recorded by the OBS when Typhoon Shanshan was passing over the OBS, we derived very high coherence (Fig. 9), suggesting that the ground motions in both SPDF and LPDF bands are mostly a response of pressure sources near the OBS, instead of being excited in regions far away. When there was no typhoon, the coherence in the LPDF band dropped from 0.9 to 0.6 while the SPDF band remained high, suggesting that the LPDF was excited at least one wavelength away in far distances, while the SPDF microseisms were excited locally, consistent with previous observations by Bromirski et al. (2005).

Discussion and conclusions

The 0.0625 Hz ocean swells traveling from opposite directions can superpose and generate 0.125 Hz standing waves, which then couple with the seafloor and propagate as seismic waves (Longuet-Higgins 1950; Kedar and Webb 2005; Webb 2007). Using the waveforms collected by land and ocean bottom seismic stations, which were very close to the path of Typhoon Shanshan, we have documented at least two source regions: one trailing after the typhoon and another near the coast at shallow water depth (Fig. 10). These unique observations are consistent with previous studies that predict these results theoretically (Longuet-Higgins 1950; Tabulevich 1992; Ponomaryov et al. 1998) or using advanced data processing techniques on waveforms collected far away from the typhoon (Gerstoft et al. 2008; Hetzer et al. 2008).

The OBSs recorded stronger signals than the land stations. The OBSs sitting on soft sediment can record stronger signals than land stations (Fig. 2). The peak amplitude at S004 occurred a few hours after the typhoon center passed over the OBS. Compared with station S004 at 5 km water depth, station S002 at 1 km water depth recorded stronger ground motions, possibly related to the evanescent nature of the acoustic waves in the water
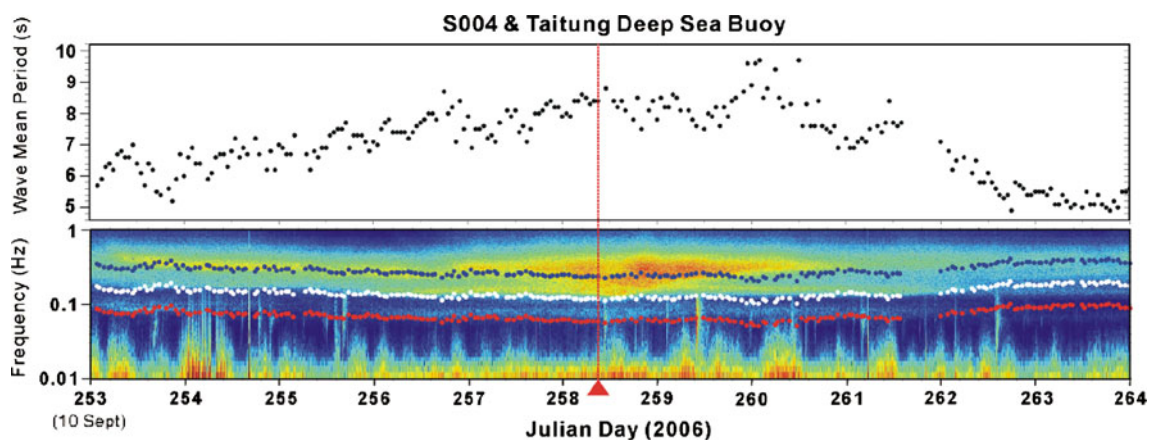
Fig. 8 Wave mean periods and frequencies (made by using a reciprocal of wave mean period to get the frequency.) recorded by the Taitung deep sea buoy near OBS station S004 (see Fig. 1 for location). The frequencies were plotted on top of the spectrogram of ground motions recorded at S004. *Red dots* are the single-frequency microseisms, while white and *blue dots* are LPDF and SPDF microseisms, respectively. There is a correlation between the power spectral densities (PSD) of LPDF band and ocean wave frequency. We found increasing period as the typhoon approached the OBS and the buoy, consistent with the results from WWIII data (Fig. 4b) and the spectrograms derived from the seismic waveforms. *Red triangle* and *dotted line* point out the time that Typhoon Shanshan was closest to S004
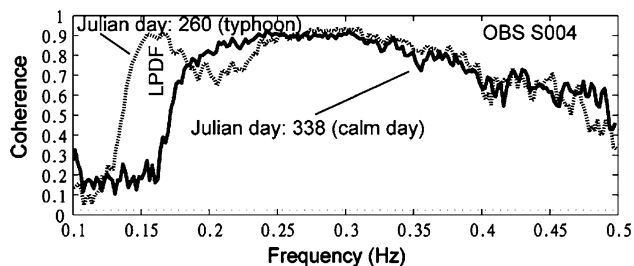
Fig. 9 Using the pressure and vertical component waveforms recorded by OBS S004 under a water depth of 4726 m, we have calculated the coherence between these two time series as a function of frequency. High coherence (> 0.8) means that most of the vertical component of ground motions was excited locally by the pressure waves in the water column. During the typhoon day (Julian day 260) and a calm day (Julian day 338), we found high coherence in the 0.23–0.33 Hz band, which is part of the SPDF band (0.20–0.45 Hz). We interpret that these are excited locally. When typhoon was over the OBS S004, we also have high coherence in the LPDF band, suggesting that the LPDF was excited locally near the typhoon. During the calm day, there is very low coherence in the LPDF band, suggesting that the source regions are far away, possibly from the coastline elsewhere as proposed by Bromirski et al. (2005)

column. However, these amplitude variations might also relate to local site effects.

Compared with station S004, station S002 recorded stronger ground motions (bigger amplitudes) and more long-period noises. However, Typhoon Shanshan passed both of the OBSs in a day. The intensity of Typhoon Shanshan did not differ much during the time period it passed over the OBSs at S002 and S004, respectively. This shows that the strength of a typhoon is not the main cause of the differences of amplitudes in this case. Possible causes include the depth difference and local site effects.

We hope to see if we can use on-land seismic data, OBS data, and ocean buoy data to study the source parameters of the typhoon. To seismically monitor the typhoon, it will be interesting to test if we can estimate roughly the source distance between the typhoon and the OBS. We derived empirical relations between the ground motions at S004 and the distance from the station to the typhoon, i.e. source distance (Fig. 11). We calculated the ratio of power

spectral density (PSD) of 0.1–0.2 Hz (LPDF band) and 0.05–0.1 Hz (single-frequency band) in the OBS displacement waveforms, and we found there is a correlation between the ratio of PSDs and the source distances from the station to the center of typhoon. Some of the outliers occurred when the typhoon turned, changed speed, or varied its intensity, and became the indicators of changes in the wave-wave interaction region while the typhoon is changing speed or direction, or making landfall and re-entering the ocean. Similar outliers can also be found, although less clear, using just the LPDF without being normalized by the single-frequency band. These changes interrupt the previously established wave-wave interaction patterns in the source regions and thus generate a new microseismic pattern. These changes may also alter the energy ratio between LPDF and single-frequency bands. So the jumping of the *en enchelon* pattern and the abrupt changes of that ratio can be used to monitor the turning of a typhoon in near real time.

Aster et al. (2008, 2010) and Bromirski and Kossin (2008) have demonstrated that it is possible to use available seismograms to study historic trends of extreme tropical cyclones and their implication in terms of global warming. Lessons learned from this study can also be applied to seismic waveforms recorded before the satellite era to study decadal-scale climate changes.

In sum, we have studied the possibility of seismically monitoring the turning of a typhoon. We observed *en echelon* patterns, which may signal starting of new sets of swells and also new wave-wave interaction patterns when the typhoon is changing direction or speed. The energy levels of the single-frequency and LPDF microseisms also change when the typhoon is turning, providing additional criteria to detect turning of the typhoon.

Satellite images provide important information on the location of the typhoon when the satellite passes over the typhoon. Seismology provides an independent and complementary method that can be used to study the typhoon in real time. In the future we may use land and cabled ocean-bottom broadband seismometers to monitor such changes

Fig. 10 There are at least 2 source regions of microseisms recorded by the OBSs and on-land stations: 1. Near the typhoon: possibly behind the tail of the typhoon because that is where the OBSs recorded strongest ground motions (Figs. 2, 5). 2. Near the coast: the coastal seismic stations recorded much stronger typhoon-related ground motions than the inland station, as seen in Fig. 4
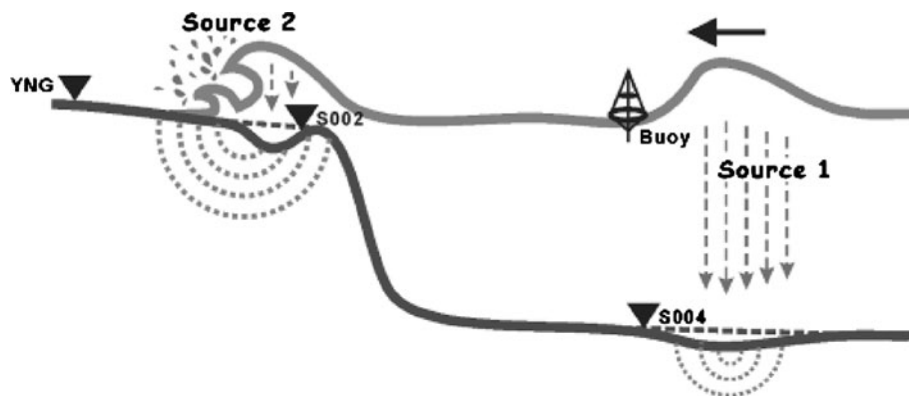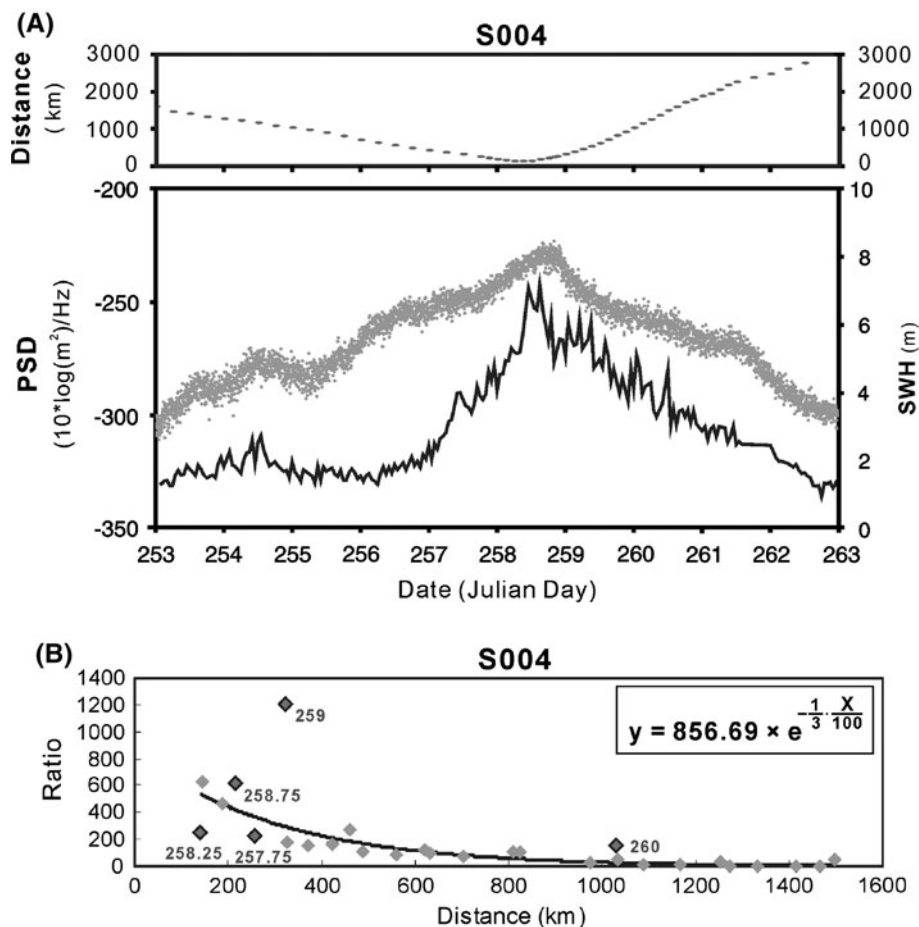
Fig. 11 Empirically derived source distance from the typhoon to OBS S004 using the energy ratio between the 5–10 s (0.1–0.2 Hz: SPDF microseisms) bands. **A** Power spectral densities (PSD) of 0.05–0.1 Hz band (*dots*) and significant wave height recorded by the Taitung deep sea buoy (*black line*). Note that the PSD of 0.1–0.2 Hz band anti-correlates with the epicentral distance. The black line depicts the significant wave height (SWH) data recorded by the nearby Taitung deep sea buoy, which correlates with the energy level of the 0.1–0.2 Hz band. **B** Determination of the source distance using the ratio (*y*) between the two bands shown in Fig. 11a, which decays exponentially as the cube of the distance (*x*) increases (see the regression equation at the upper right corner). The *numbers* depict the Julian days of the outliers. The outliers occurred when the speed or the direction of the typhoon changed, except when part of the typhoon made landfall, or moved to shallow water regions. (c.f. Fig. 1)

in real time. Because all the seismic waveforms are readily available, such a practice will be relatively inexpensive and can provide additional information to the more traditional typhoon alarm systems.

References

Aster R, McNamara D, Bromirski P (2008) Multi-decadal climate-induced variability in microseisms. Seismol Res Lett 79(2): 194–202. doi:10.1785/gssrl.79.2.194

Aster R, McNamara D, Bromirski PD (2010) Global trends in extremal microseism intensity. Geophy Res Lett 37:L14303. doi:10.1029/2010GL043472

Bromirski PD (2001) Vibrations from the "perfect storm". Geochem Geophys Geosyst 2 (paper number 2000GC000119)

Bromirski PD, Duennebier FK (2002) The near-coastal microseism spectrum: spatial and temporal wave climate relationships. J Geophys Res 107(B8):2166. doi:10.1029/2001JB000265

Bromirski PD, Gerstoft P (2009) Dominant source regions of the Earth's "hum" are coastal. Geophys Res Lett 36. doi:10.1029/2009GL038903

Bromirski PD, Kossin JP (2008) Increasing hurricane wave power along the U.S. Atlantic and Gulf coasts. J Geophys Res 113:C07012. doi:10.1029/2007JC004706

Bromirski PD, Flick RE, Graham N (1999) Ocean wave height determined from inland seismometer data: implications for investigating wave climate changes in the NE Pacific. J Geophys Res 104(C9):20753–20766

Bromirski PD, Duennebier FK, Stephen RA (2005) Mid-ocean microseisms. Geochem Geophys Geosyst 6:Q04009. doi:10.1029/2004GC000768

Cessaro RK (1994) Sources of primary and secondary microseisms. Bull Seismol Soc Am 84:142–148

Chevrot S, Sylvander M, Benahmed S, Ponsolles C, Lefe've JM, Paradis D (2007) Source locations of secondary microseisms in western Europe: evidence for both coastal and pelagic sources. J Geophys Res 112:B11301. doi:10.1029/2007JB005059

Chi WC, Chen WJ, Dolenc D, Kuo BY, Liu CR, Collins J (2010) Seismological records of the 2006 Typhoon Shanshan that lits up seismic stations along its way. Seismol Res Lett 81(e):592–596. doi:10.1785/gssrl.81.4.592

Collins JA, Vernon FL, Orcutt JA, Stephen RA (2002) Upper mantle structure beneath the Hawaiian swell: constraints from the ocean seismic network pilot experiment. Geophys Res Lett 29(11):17.1–17.4

Crawford WC (2000) Seafloor compliance measurements: applications for hydrocarbon exploration. Lithos Sci Rep 2:151–156

Crawford WC (2004) The sensitivity of seafloor compliance measurements to sub-basalt sediments. Geophys J Int 157:1130–1145

Crawford WC, Webb SC, Hildebrand JA (1991) Seafloor compliance observed by long-period pressure and displacement measurements. J Geophys Res 96:16151–16160

Essen HH, Krüger F, Dahm T, Grevemeyer I (2003) On the generation of secondary microseisms observed in northern and central Europe. J Geophys Res 108:2506–2520. doi:10.1029/2002JB002338

Friedrich A, Kruger F, Klinge K (1998) Ocean-generated microseismic noise located with the Graffenberg array. J Seismol 2:47–64. doi:10.1023/A:1009788904007

Gerstoft O, Fehler MC, Sabra KG (2006) When Katrina hit California. Geophys Res Lett 33:L17308. doi:10.1029/2006GL027270

Gerstoft P, Shearer PM, Harmon N, Zhang J (2008) Global P, PP, and PKP wave microseisms observed from distant storms. Geophys Res Lett 35:L23306. doi:10.1029/2008GL036111

Hetzer CH, Waxler R, Gilbert K, Talmadge CL, Bass HE (2008) Infrasound from hurricanes: dependence on the ambient ocean surface wave field. Geophys Res Lett 35:L14609. doi:10.1029/2008GL034614

Hoyois P, Below R, Scheuren JM, Guha-Sapir D (2007) Annual disaster statistical review: numbers and trends, 2006. Center for Research on the Epidemiology of Disasters, School of Public Health, Catholic University of Louvain, Brussels

Kedar S, Webb FH (2005) The ocean's seismic hum. Science 307(5710):682–683. doi:10.1126/science.1108380

Kedar S, Longuet-Higgins M, Webb F, Graham N, Clayton R, Jones C (2008) The Origin of deep ocean microseisms in the North Atlantic Ocean. Proc R Soc Lond A 464:777–793. doi:10.1098/rspa.2007.0277

Koper KD, de Foy B (2008) Seasonal anisotropy in short-period seismic noise recorded in South Asia. Bull Seismol Soc Am 98(6):3033–3045. doi:10.1785/0120080082

Kuo BY, Chi WC, Lin CR, Chang ETY, Collins J, Liu CS (2009) Two-station measurement of Rayleigh-wave phase velocities for the Huatung basin, the westernmost Philippine Sea, with OBS: implications for regional tectonics. Geophys J Int 179:1859–1869. doi:10.1111/j.1365-246X.2009.04391.x

Landes ML, Hubans F, Shapiro NM, Paul A, Campillo M (2010) Origin of deep ocean microseisms by using teleseismic body waves. J Geophys Res 115:B05302. doi:10.1029/2009JB006918

Lang S, Pierce H (2006) Super Typhoon Cimaron. SSAI/NASA GSFC. http://earthobservatory.nasa.gov/NaturalHazards/view.php?id=17542. October 31, 2006

Lin CH, Hsu LW, Ho MY, Shin TC, Chen KJ, Yeh YH (2007) Low-frequency submarine volcanic swarms at the southwestern end of the Okinawa Trough. Geophys Res Lett 34:L06310. doi:10.1029/2006GL029207

Lin CR, Kuo BY, Liang WT, Chi WC, Huang YC, Collins J, Wang CY (2009) Ambient noise and teleseismic signals recorded by ocean-bottom seismometers offshore Eastern Taiwan. Terr Atmos Ocean Sci 21(5):743–755. doi:10.3319/TAO.2009.09.14.01(T)

Longuet-Higgins M (1950) A theory of the origin of microseisms. Philos Trans R Soc Lond A 243:1–35

NOAA/NCEP et al. (2010) http://polar.ncep.noaa.gov/waves/index2.shtml. 11 Feb 2010 EST

Ponomaryov EA, Sorokin AG, Tabulevich VN (1998) Microseisms and infrasound: a kind of remote sensing. Phys Earth Planet Int 108:339–346

Rhie J, Romanowicz B (2006) A study of the relation between ocean storms and the Earth's hum. Geochem Geophys Geosyst 7:A10004. doi:10.1029/2006GC001274

Stehly L, Campillo M, Shapiro NM (2006) A study of the seismic noise from its long-range correlation properties. J Geophys Res 111:B10306. doi:10.1029/2005JB004237

Stephen RA, Duennebier FK, Harris D, Jolly J, Bolmer ST, Bromirski PD (2003) Data report: broadband seismic observations at the HAWAII-2 Observatory. In: Kasahara J, Stephen RA, Acton GD, Frey FA (eds) Proceedings of the ocean drilling program, scientific results 200, pp 1–63. [Online]. Available from World Wide Web: http://www-odp.tamu.edu/publications/200_SR/VOLUME/CHAPTERS/003.PDF [Cited 201010-16]

Suda N (1998) Earth's background free oscillations. Science 279:2089. doi:10.1126/science.279.5359.2089

Sutton GH (1996) Ocean bottom microseisms from a distant supertyphoon. Geophys Res Lett 23(5):499–502

Tabulevich VN (1971) The effect of the velocity of the centre of a cyclone on the generation of microseisms. Pure Appl Geophys 85(1):69–74. doi:10.1007/BF00875399

Tabulevich VN (1992) Microseismic and infrasound waves. In: Research reports in physics. Springer, Berlin

Tanimoto T (2008) Humming a different tune. Nature 452:539–541. doi:10.1038/452539a

Thwaites FT, Wooding FB, Ware JD, Peal KR, Collins JA (2005) A leveling system for an ocean-bottom seismometer. MTS/IEEE 2:1268–1272. doi:10.1109/OCEANS.2005.1639929

Tolman HL (2005) Manual and wave user system documentation of WAVEWATCH-III > NOAA, Camp Springs, MD (available at http://polar.ncep.noaa.gov/)

Wang JH, Chi WC, Edwards RN, Willoughby EC (2010) Effects of sea states on seafloor compliance studies. Mar Geophys Res doi:10.1007/s11001-010-9091-z

Webb S (2007) The earth's 'hum' is driven by ocean waves over the continental shelves. Nature 445:754–756. doi:10.1038/nature 05536

Willoughby EC (2003) Resource evaluation of marine gas hydrate deposits using the seafloor compliance method: experimental methods and results. Ph.D. thesis, University of Toronto

Willoughby EC, Edwards RN (1997) On the resource evaluation of marine gas-hydrate deposits using seafloor compliance methods. Geophys J Int 131:751–766

Willoughby EC, Latychev K, Edwards RN, Mihajlovic G (2000) Resource evaluation of marine gas hydrate deposits using seafloor compliance methods. In: Holder GD, Bishnoi PR (eds) Gas hydrates: challenges for the future. The New York Academy of Science, New York, pp 146–158

Willoughby EC, Latychev K, Edwards RN, Schwalenberg K, Hyndman RD (2008) Seafloor compliance imaging of marine gas hydrate deposits and cold vent structures. J Geophys Res 113:B07107. doi:10.1029/2005JB004136

Wilson JD, Makris NC (2008) Quantifying hurricane destructive power, wind speed, and air-sea material exchange with natural undersea sound. Geophys Res Lett 35:L10603. doi:10.1029/2008 GL033200

Wilson DK, Frisk GV, Lindstrom TE, Sellers CJ (2003) Measurement and prediction of ultralow frequency ocean ambient noise off the eastern U.S. coast. J Acous Soc Am 113(6):3117–3133

Yamamoto T, Torii T (1986) Seabed shear modulus profile inversion using surface gravity (water) wave-induced bottom motion. Geophys J Int 85:413–431

Zhang J, Gerstoft P, Bromirski PD (2010) Pelagic and coastal sources of P-wave microseisms: generation under tropical cyclones. Geophys Res Lett 37:L15301